RSC Advances

PAPER

View Article Online
View Journal | View Issue

Cite this: *RSC Adv.*, 2021, **11**, 7

Integrated Cr and S poisoning of a $La_{0.6}Sr_{0.4}Co_{0.2}Fe_{0.8}O_{3-\delta}$ (LSCF) cathode for solid oxide fuel cells†

Cheng Cheng Wang,[ab] Mortaza Gholizadeh,[c] Bingxue Hou[d] and Xincan Fan*[a]

Received 30th October 2020
Accepted 17th November 2020

DOI: 10.1039/d0ra09239h

rsc.li/rsc-advances

Strontium segregation in a $La_{0.6}Sr_{0.4}Co_{0.2}Fe_{0.8}O_{3-\delta}$ (LSCF) electrode reacts with Cr and S in a solid oxide fuel cell (SOFC), which can cause cell performance deterioration. Integrated Cr and S poisoning for LSCF cathodes of SOFC was studied at 800 °C of 200 mA cm^{-2} (cathodic) for 20 h. After polarization in Cr and S at 800 °C for 20 h, polarization and ohmic resistances for LSCF were 2.4 Ω cm^2 and 3.4 Ω cm^2, which were larger than those for LSCF electrodes after Cr deposition only and S deposition only, respectively. The results illustrated that Cr and S deposition occurred on the surface of LSCF, which could form $SrCrO_4$ and $SrSO_4$. Compared to Cr deposition only and S deposition only, integrated Cr and S deposition was unsystematic, and the degradation phenomenon of Cr and S poisoning was more severe. The integrated Cr and S deposition of the LSCF electrodes was induced *via* interactions among CrO, SO_2 and segregated SrO from LSCF.

1. Introduction

A solid oxide fuel cell (SOFC) is a new type of power generation device, which converts chemical energy into electrical energy with high efficiency and low pollutant emission.[1] $La_{0.6}Sr_{0.4}Co_{0.2}Fe_{0.8}O_{3-\delta}$ (LSCF)[2] has been extensively studied and regarded as the most promising cathodes for IT-SOFCs[3] due to its good mixed electronic and ionic conductivities and O_2 reduction reaction catalytic activity.[4] However, despite the excellent activity of LSCF, one of the obstacles for the wide commercialization of SOFCs is the chemical instability on the surface and at the triple-phase boundaries (TPBs) of cathodes and cathode contamination, such as Cr and S, which can be either from the volatile species of metallic interconnect[2] or in the air stream.[5] It was reported that particularly sulfur could deposit at the cathode side, poisoning and degrading the cell performance, while the formation of secondary phases, such as $SrSO_4$ and $CoFe_2O_4$, was also observed.[6] Some studies showed that a two-step degradation was observed; the first rapid stage step was contributed to the fast SO_2 adsorption, and the second gradual degradation stage step was related to the formation of $SrSO_4$. The formation of $CoFe_2O_4$ and $La_2O_2SO_4$ was also reported with the help of a thermodynamical calculation, particularly for a high SO_2 partial pressure.[7]

Some studies have shown that the durability for SOFC stacks exhibited an interesting degradation phenomenon.[8] The majority of impurities affecting the performance could be attributed to Cr and S for cathodes,[9] while P and S for anodes.[10] Regarding the Cr poisoning mechanism, numerous results have reported that Cr deposited on the electrode surface or interface, causing the degradation in the performance of the LSCF cathodes.[11] Although a few disagreements still exist on the Cr deposition mechanism,[12] extensive evidences showed that Cr deposition was only a chemical reaction induced by nucleating agents,[12] which was related to the segregation as well as migration of cationic species on the surface of perovskites.[13] Interestingly, there are still a few reports focusing on combining the degradation phenomenon of SOFC cathodes.

The effect of integrated Cr and S on the electrochemical performance of LSM cathodes was studied at 800 °C,[14] and it led to the formation of $SrCrO_4$ and $SrSO_4$. The deposition was mainly due to a chemical reaction among Cr, S and SrO. Bo Wei *et al.*[18] even studied the effect of Cr deposition on LSCF electrodes under SOFC and SOEC modes. Their results showed that the electrochemical performance of LSCF electrodes for the O_2 reduction reaction (ORR) under the solid oxide fuel cell (SOFC) mode and for the O_2 evolution reaction (OER) under the solid oxide electrolysis cell (SOEC) mode severely decreased after an exposure to Cr-containing air at open circuit voltage. They obtained the conclusion that $SrCrO_4$ and deposition of a ~1 μm thick Cr deposit layer limited the oxygen exchange and the diffusion related processes. However, the effect of Cr and S on the electrochemical performance of LSCF has not been

[a]Shen Zhen Polytechnic, Shenzhen, 518055, China. E-mail: horsefxc@szpt.edu.cn
[b]Fuels and Energy Technology Institute, Department of Chemical Engineering, Curtin University, Perth, WA 6102, Australia
[c]Faculty of Chemical and Petroleum Engineering, University of Tabriz, Tabriz, Iran
[d]Aviation Engineering Institute, Civil Aviation Flight University of China, GuangHan, 618037, China

† Electronic supplementary information (ESI) available. See DOI: 10.1039/d0ra09239h

investigated yet. Hence, in this study, the combination of Cr and S poisoning on LSCF electrodes was studied at 800 °C. It showed that the interaction among Cr, S and LSCF caused the formation of $SrCrO_4$ and $SrSO_4$ on the surface of LSCF. The deposition at the LSCF electrodes was controlled by a chemical reaction among Cr, S and SrO.

2. Experimental

$Gd_{0.1}Ce_{0.9}O_{1.95}$ (GDC, fuel cell materials) and $La_{0.6}Sr_{0.4}Co_{0.2}Fe_{0.8}O_3$ (LSCF, fuel cell materials) powders were used in this study. The half-cell preparation method was listed in previously published paper.[15] A certain amount of GDC pellets were weighed, pressed and fired at 1450 °C for 5 h (0.5–0.9 mm thickness, and 20 mm diameter). Then, organic inks were mixed with LSCF powders (in a 50 : 50 weight ratio) to obtain slurries. The organic ink was made of ethyl cellulose as the binder and terpineol as the solvent. Then, it was sprayed onto the surface of GDC (0.5 cm^2), and the half-cells were sintered at 1100 °C for 2 h.

The electrochemical performance of the half cells was tested by the three electrode method.[16] In order to study the effect of Cr poisoning on SOFC cathode materials, and also simulate the real SOFC testing condition, Fe–Cr alloy was used in this study. Fe–Cr alloy (RA446) was used as a coupon with channels (1.2 × 1.2 mm). Then, Fe–Cr was put onto the LSCF electrode.[17] Dry SO_2-containing (1 ppm) air (100 mL min^{-1}) was flowed into cathode side.

A Gamry Reference 3000 Potentiostat was used to test the polarization and the impedance curve of the cells at 800 °C. Impedance data were obtained from 0.1 Hz to 100 000 Hz under OCV conditions to get the ohmic resistances (R_Ω) and electrode polarization resistances (R_E) at different frequencies.

XRD (Bruker D8 Advances) was used to test the structure of cells before and after poisoning. An XPS ESCALAB 250Xi instrument (Thermo Fisher) was used to analyze the element valence. The microstructural change of LSCF electrodes was detected by SEM and mapping from a NEON 40EsB. Sulfur deposition in LSCF electrodes was further studied by the FIB-STEM technique. A protective layer of Pt was deposited onto the surface before the ion beam milling. The TEM specimen was then transferred onto a Cu grid. Then, the final step was the polishing using an ion beam. Both the spectra mode and fast imaging mode were integrated to analyze the sulfur deposition in LSCF electrodes by the TOF-SIMS technique (PHI NanoTOFII).

3. Results and discussion

3.1 Electrochemical performance of LSCF electrodes

Fig. S1† shows the polarization and impedance curves of the O_2 reduction reaction on the LSCF electrode in ambient air as

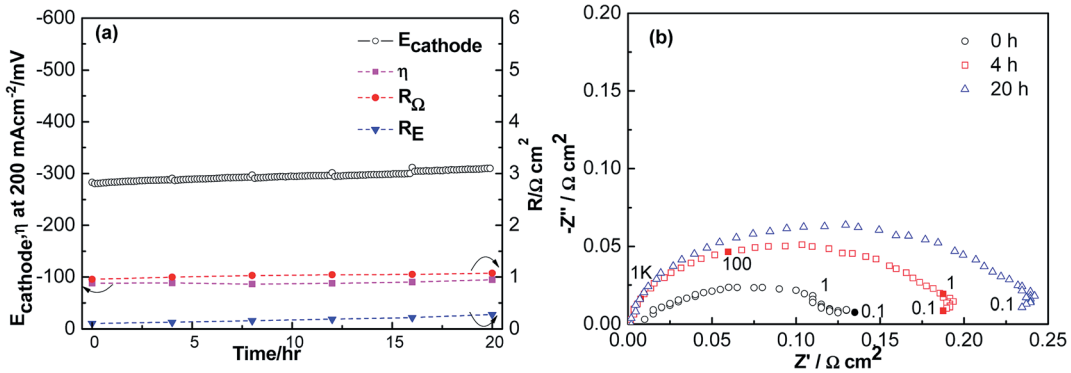

Fig. 1 Polarization (a) and impedance curves (b) of porous LSCF cathodes in the presence of 1 ppm SO_2 at a cathodic current of 200 mA cm^{-2} for 20 h at 800 °C.

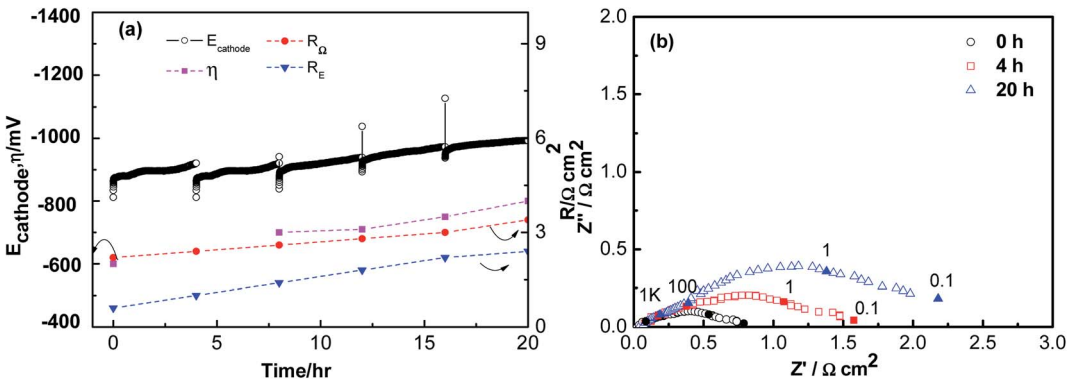

Fig. 2 Polarization (a) and impedance curves (b) of porous LSCF cathodes in the presence of the Fe–Cr alloy and 1 ppm SO_2 at a cathodic current of 200 mA cm^{-2} for 20 h at 800 °C.

a function of the polarization time at 200 mA cm^{-2} for 20 h at 800 °C. According to Fig. S1a,† it can be seen that $E_{cathode}$ was around 225 mV after being polarized for 20 h. Fig. S1b† shows that R_E was 0.12 Ω cm^2 and it changed to 0.15 Ω cm^2 after being polarized for 20 h. The value was also stable, which was similar to the change of $E_{cathode}$. Moreover, ohmic resistance (R_Ω) was around 1.7 Ω cm^2 after 20 h.

Fig. S2† shows the polarization and impedance curves of the O_2 reduction reaction on the LSCF electrode in the presence of a Fe–Cr alloy interconnect as a function of the polarization time under a cathodic current passage at 200 mA cm^{-2} for 20 h at 800 °C. R_Ω gradually increased from 2.25 Ω cm^{-2} to 3.19 Ω cm^{-2}; while electrode polarization resistance (R_E) increased from 0.5 Ω cm^{-2} to 1.8 Ω cm^{-2} after being polarized for 20 h. All these results indicated that the increase in R_Ω was due to the formation of a resistive chromium oxide scale and Cr deposition at the LSCF electrode surface, which was in accordance with Bo Wei's results.[18] The increase in R_E illustrated that the presence of Cr species had a significant effect on the oxygen exchange, and the diffusion process generally associated with the electrode low frequencies.[19]

Fig. 1 shows the polarization and the impedance curves for ORR on the LSCF electrode as a function of polarization time at 200 mA cm^{-2} in the presence of 1 ppm SO_2 at 800 °C for 20 h. At 800 °C, $E_{cathode}$ was stable, except for a small decrease from 250 to 215 mV initially (Fig. 1a). Initial R_E was 0.13 Ω cm^2, and it increased to 0.19 Ω cm^2 (Fig. 1b). Compared to the change in the potential and polarization resistance in ambient air, the difference in the change of $E_{cathode}$ was a clear indication of the poisoning effect of sulfur on the LSCF electrode for the O_2 reduction reaction.

Fig. 2 shows the polarization and impedance curves for ORR on the LSCF electrode as a function of polarization time at 200 mA cm^{-2} in the presence of integrated Cr and S poisoning at 800 °C for 20 h. $E_{cathode}$ increased from 0.8 V to 1.0 V, and the increase correlated with Cr and S poisoning phenomenon of the LSCF electrode. R_E was 0.6 Ω cm^2, and increased to 2.4 Ω cm^2 after 20 h. Moreover, R_Ω increased from 2 Ω cm^2 to 3.4 Ω cm^2. It

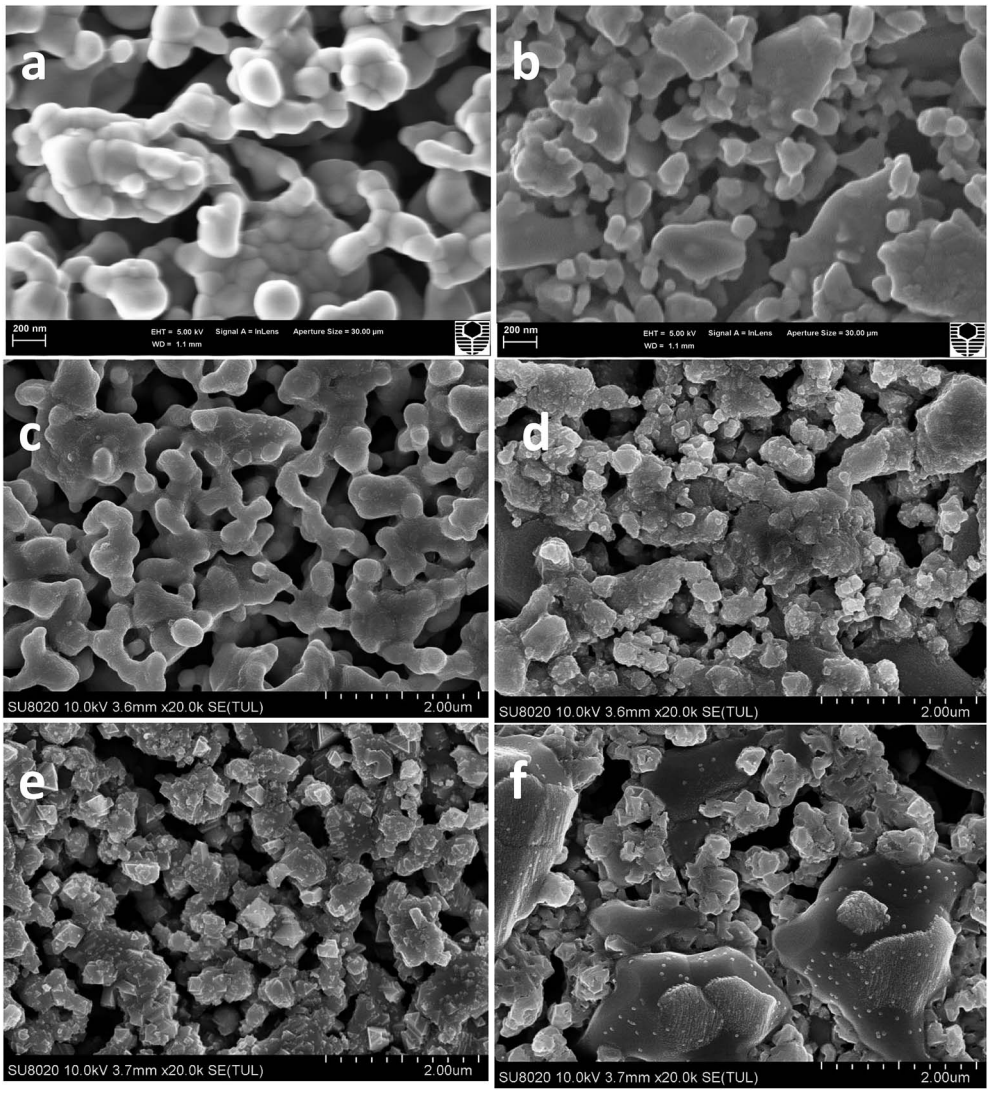

Fig. 3 Surface of SEM micrographs of LSCF cathodes at a cathodic current of 200 mA cm^{-2} in the ambient air (a), presence of 1 ppm SO_2 (b), presence of the Fe–Cr alloy ((c)-channel, (d)-rib), presence of the Fe–Cr alloy and 1 ppm SO_2 ((e)-channel, (f)-rib) at 800 °C for 20 h.

is also indicated in Fig. 4 that the increase in R_E was also higher than that of the Cr deposition only and S deposition only. Moreover, $E_{cathode}$ increased more obviously, illustrating that the more severe Cr and S poisoning phenomenon of the LSCF electrodes.

3.2 Microstructure change of LSCF electrodes

Fig. 3 shows the SEM images of the surface of the LSCF cathodes at 200 mA cm^{-2} in ambient air (a), S poisoning condition (b), Fe–Cr poisoning condition ((c)-channel, (d)-rib), integrated Cr and S poisoning condition ((e)-channel, (f)-rib) at 800 °C for 20 h. For LSCF electrodes polarized in ambient air, the particle size of LSCF was around 200 nm, and the particles were smooth (Fig. 3a). After being polarized at 200 mA cm^{-2} in the presence of 1 ppm SO_2 for 20 h at 800 °C (Fig. 3b), the microstructure change of the surface of LSCF electrodes was small, although there were a few isolated small particles with diameter of 50–80 nm on the LSCF surface. In Fig. 3c and d, the LSCF particles were rough, and more irregular particles were dispersed on the surface, particular in the rib area. In Fig. 3e and f, irregular tiny particles (10–20 nm) and large spinel particles (100–200 nm) were observed for LSCF electrodes after being poisoned. It can be concluded that there was a more severe poisoning in the rib than those observed in the channel area.

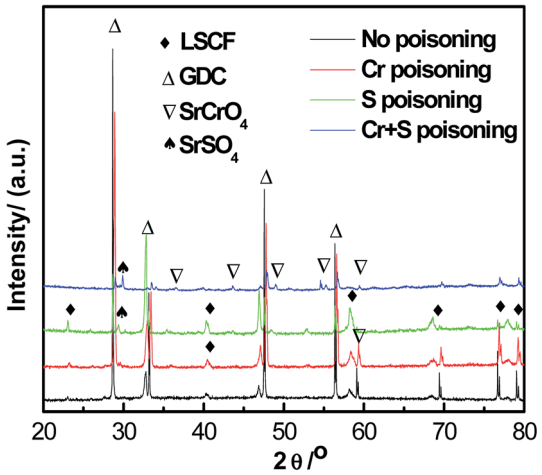

Fig. 5 XRD patterns of LSCF cathodes at a cathodic current of 200 mA cm^{-2} at 800 °C in the ambient air (a), presence of Fe–Cr alloy (b), presence of the Fe–Cr alloy and 1 ppm SO_2 (d), presence of 1 ppm SO_2 (c) at 800 °C for 20 h.

Fig. S3† shows SEM images of the cross section of the LSCF cathodes at 200 mA cm^{-2} in ambient air (a), S poisoning condition (b), Fe–Cr poisoning condition ((c)-channel, (d)-rib), integrated Cr and S poisoning condition ((e)-channel, (f)-rib)

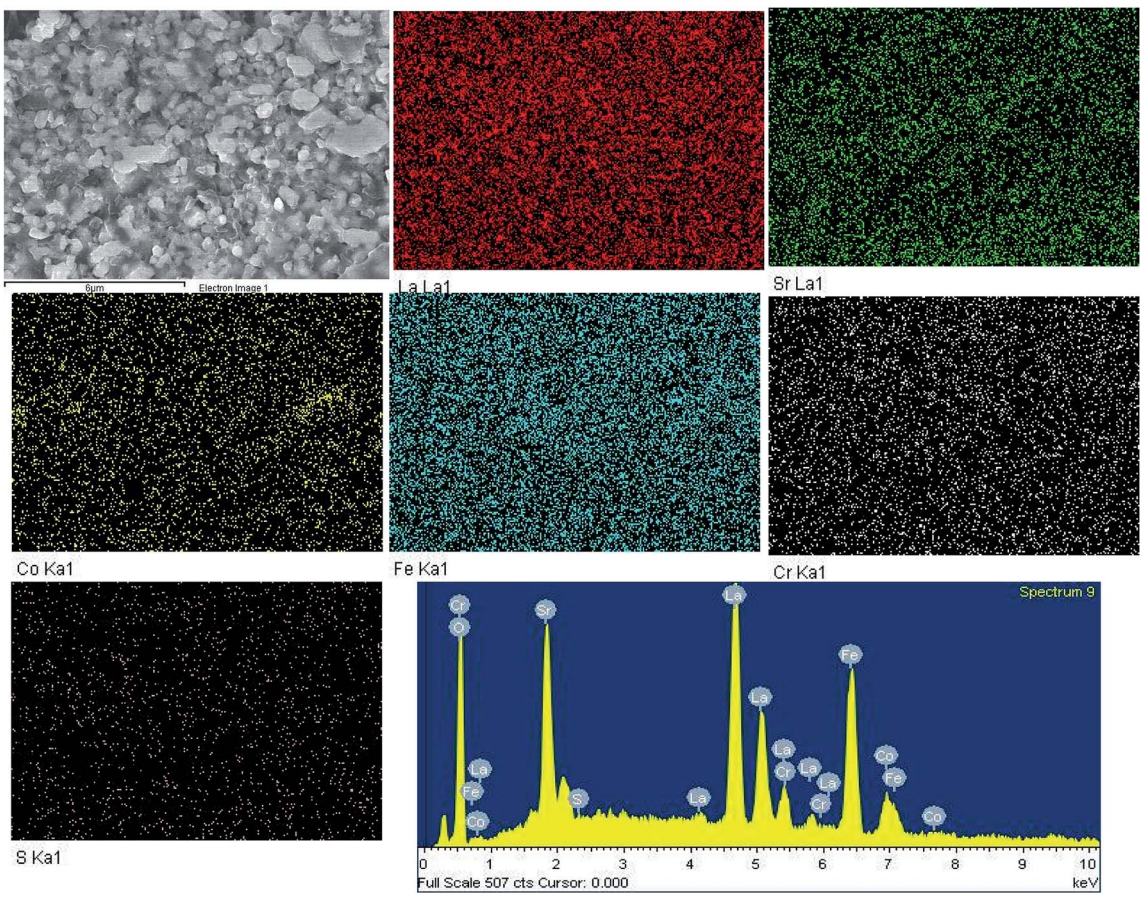

Fig. 4 Cross sectional mapping and EDX of SEM micrographs of LSCF cathodes at a cathodic current of 200 mA cm^{-2} in the presence of the Fe–Cr alloy and 1 ppm SO_2 at 800 °C for 20 h.

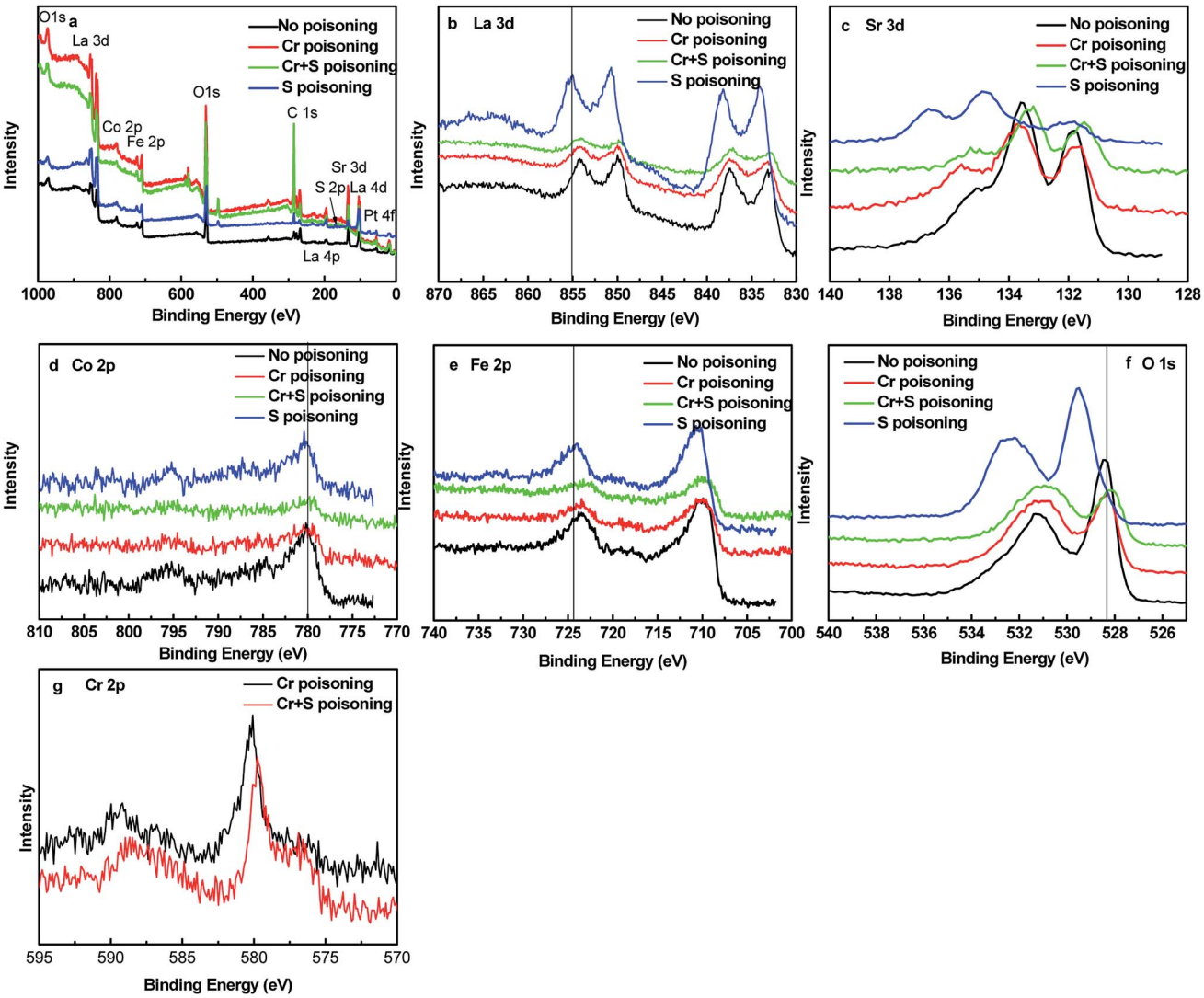

Fig. 6 High resolution XPS spectrum of La3d, Sr3d, Co, Fe as well as Cr2p for the surface of LSCF cathodes at a cathodic current of 200 mA cm^{-2} at 800 °C for 20 h in the presence of the Fe–Cr alloy, in the presence of 1 ppm SO_2 and in the presence of Fe–Cr alloy and 1 ppm SO_2.

at 800 °C for 20 h. From Fig. S3a,† it can be seen that there was a good contact between LSCF and GDC. After being poisoned in the presence of 1 ppm SO_2, LSCF particles were covered by a thin film. A more obvious microstructure change was observed after being exposed to the integrated Fe–Cr alloy and 1 ppm SO_2, which was similar to the above-mentioned surface SEM image results. In Fig. S3c and d,† there are some tiny round particles observed in the image; however, after LSCF electrodes were poisoned by the integrated Fe–Cr alloy and 1 ppm SO_2, some spinel particles were clearly observed, particularly in the rib section. All the surface and the cross section results clearly illustrated the more severe Cr and S poisoning of the LSCF electrodes. It is worth mentioning that as compared with the Cr poisoning phenomenon, the S poisoning effect was not that severe.

3.3 Sulfur deposition by EDS and Mapping

Fig. S4† is EDS and mapping of the cross section of LSCF electrodes after polarization under 200 mA cm^{-2} at 800 °C in 1 ppm SO_2-containing air for 20 h. A few sulfur spots were observed in the bulk of LSCF electrodes, and a few cobalt enriched particles could also be detected, which might indicate the possible formation of a Co–Fe enriched phase. Fig. S5† and 4 is the EDS and mapping of cross section of LSCF electrodes after polarization in the Fe–Cr alloy, in integrated Fe–Cr alloy and 1 ppm SO_2 for 20 h. Although the resolution of the mapping image was not that clear as compared to Fig. S4,† the EDS results clearly indicated the presence of Cr, Cr and S signals in the bulk of the LSCF electrodes.

3.4 XPS and XRD analysis of LSCF electrodes

Fig. 5 shows XRD patterns for the LSCF electrodes in ambient air, Cr poisoning, Cr and S poisoning, S poisoning after polarization at 800 °C for 20 h. For LSCF electrodes polarized in air, only LSCF and GDC peaks were detected. Both $SrCrO_4$ and $SrSO_4$ peaks were observed after Cr and S poisoning of the LSCF electrodes. Moreover, regarding the sulfur poisoning of the LSCF electrodes, a $SrSO_4$ peak appeared at around 28°.

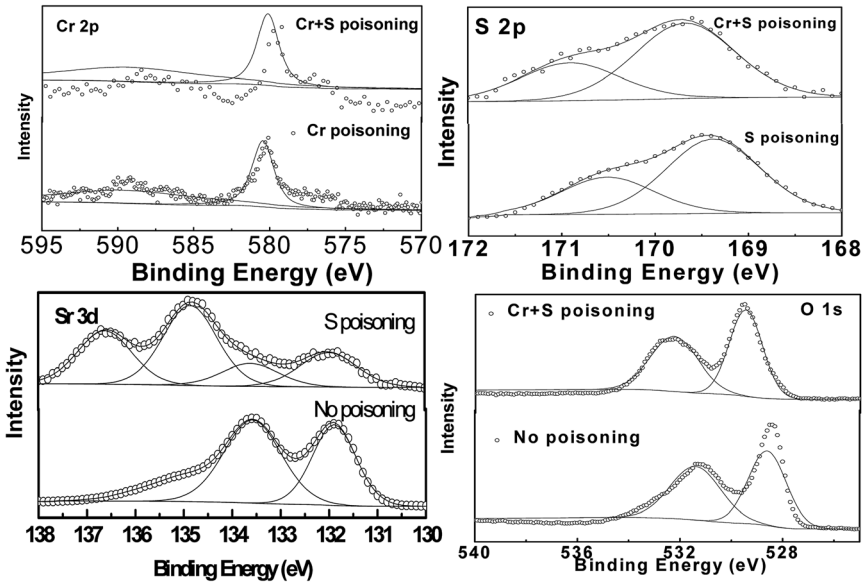

Fig. 7 Selected deconvoluted high resolution XPS spectrum of Sr3d, Cr2p, S2p and O 1s for the surface of LSCF cathodes at a cathodic current of 200 mA cm^{-2} at 800 °C for 20 h in the presence of the Fe–Cr alloy, in the presence of 1 ppm SO_2 and in the presence of the Fe–Cr alloy and 1 ppm SO_2.

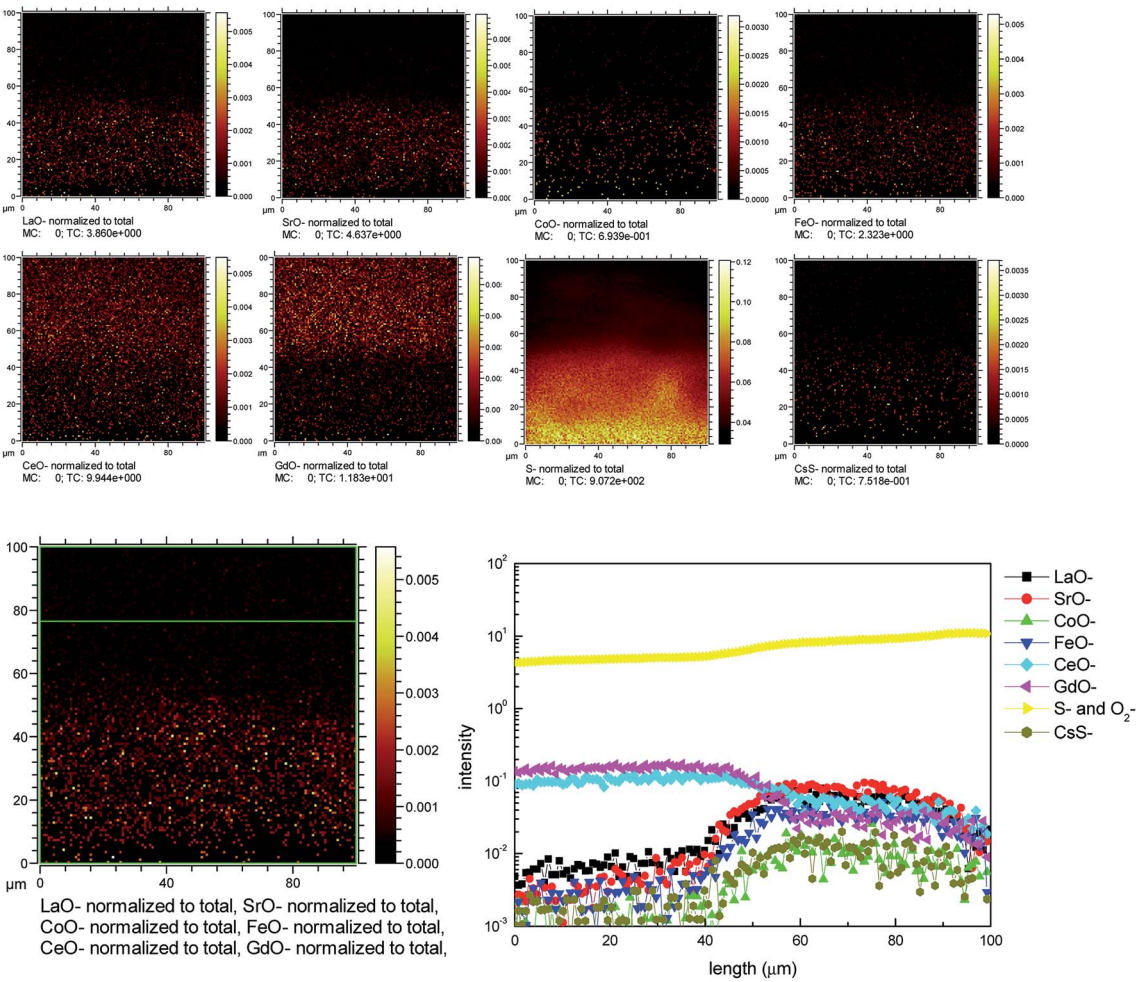

Fig. 8 TOF-SIMS of LSCF cathodes at a cathodic current of 200 mA cm^{-2} at 800 °C in the presence of 1 ppm SO_2 for 20 h.

Regarding the Cr poisoning of the LSCF electrodes, only LSCF and GDC peaks were detected.

Fig. 6 shows XPS spectra for La 3d, Sr 3d, Co 2p, Fe 2p, Cr 2p and S 2p on the surface of the LSCF electrodes of 200 mA cm^{-2} in air, Cr poisoning, Cr and S poisoning, S poisoning at 800 °C for 20 h. The binding energies of La 3d, Co 2p, Fe 2p were in accordance with each other from Fig. S6b, d and e.† Furthermore, Fig. 7 shows the deconvoluted Cr 2p, S 2p, Sr 3d and O 1s spectra. For the LSCF electrodes polarized in ambient air, an $Sr3d_{5/2}$ peak at 132.3 eV was attributed to Sr^{2+} ions in the LSCF lattice, while for the LSCF electrodes after sulfur poisoning, an $Sr3d_{5/2}$ peak appeared at 132.3 eV and 134.1 eV, which was attributed to Sr^{2+} ions and $SrSO_4$. Fig. 7b shows that the binding energy of the deconvoluted S $2p_{3/2}$ peak was 168.5 eV, and it could correspond to the S $2p_{3/2}$ of 168.5 eV for SO_4^{2-}. $SrSO_4$ was obtained after being exposed for $La_{0.6}Sr_{0.4}CoO_{3-\delta}$ to >1 ppm SO_2 for 24 h.[20] Moreover, the binding energy of Cr $2p_{1/2}$ and Cr $2p_{3/2}$ was 588.4 eV and 579.4 eV, respectively, which corresponds to Cr^{6+} compounds. Cr^{6+} compounds were identified by Cr $2p_{3/2}$ peaks ranging from 578.3 to 580.1 eV according to chemistry forms *i.e.* CrO_3, CrO_4^{2-} or CrO_7^{2-}. The dominant spectra related with Cr^{6+} indicated that Cr deposits were $SrCrO_4$.[14]

3.5. Sulfur deposition by FIB-STEM and TOF-SIMS

Fig. 8 shows the TOF-SIMS image of the LSCF electrode at the electrode/electrolyte interface at 200 mA cm^{-2} in 1 ppm SO_2-containing air for 20 h at 800 °C. The results were much clearer than that of the mapping result of the same sample. Sulfur elements were observed and distributed well in the bulk of the LSCF electrode. Fig. S6† shows the detailed process of the TEM specimen preparation using FIB-SEM. Fig. 9 shows HAADF micrographs as well as EDS elemental maps of the LSCF thin wafer sample at the electrode/electrolyte interface under 200 mA cm^{-2} in the presence of 1 ppm SO_2 for 20 h at 800 °C. Sulfur deposition was detected within the bulk of the electrodes and

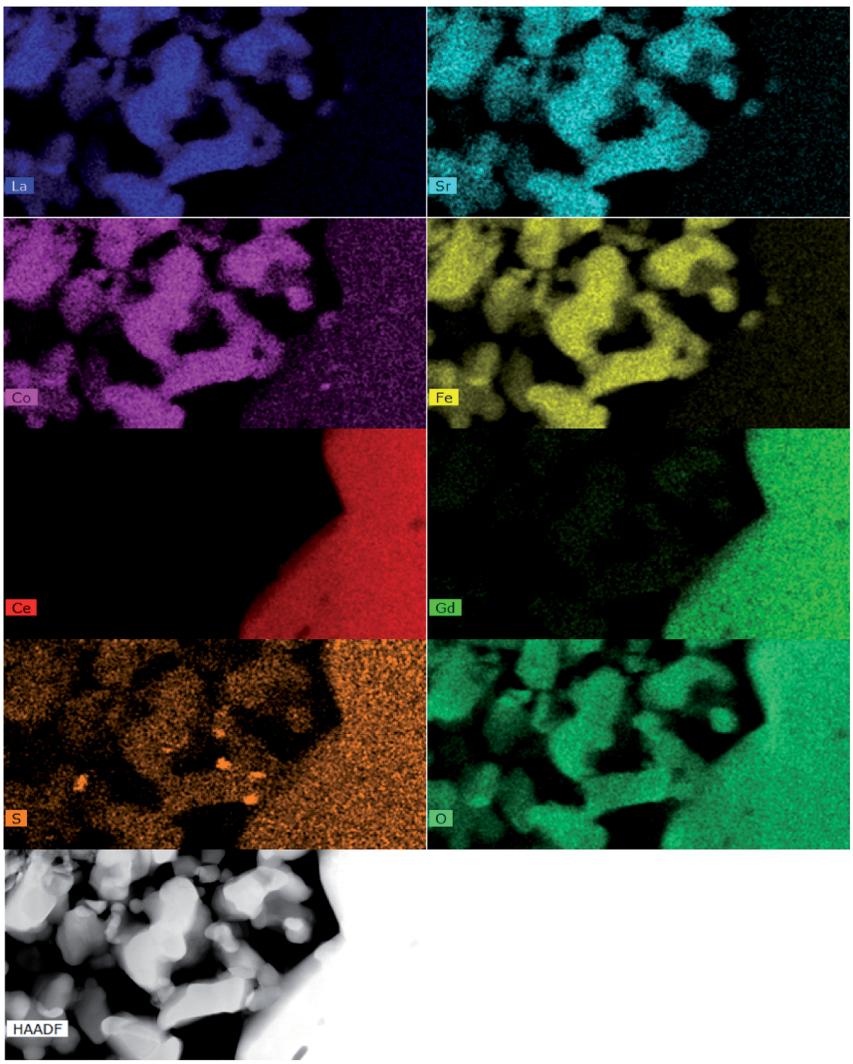

Fig. 9 HAADF micrographs and EDS elemental maps of the LSCF thin wafer sample at the electrode/electrolyte interface under cathodic current passage at 200 mA cm^{-2} in the presence of 1 ppm SO_2 for 20 h at 800 °C. The bright orange spots correspond to the sulfur element and other dark orange colors correspond to the background noise. Bar = 1 μm.

the distribution of sulfur-rich particles was not uniform. The size of the deposited sulfur particles was around 100 nm.

4. Conclusions

Integrated Cr and S deposition and poisoning on the electrochemical performance and microstructures of the LSCF cathodes were studied at cathodic conditions. TOF-SIMS and FIB-STEM results clearly showed that Cr and S depositions occurred on the surface and the bulk, forming $SrSO_4$/$SrCrO_4$ compounds, which accelerated the LSCF degradation.

Conflicts of interest

There are no conflicts to declare.

Acknowledgements

The authors acknowledge the facilities, the scientific and technical assistance of the Imaging Facility at the Centre for Microscopy, Characterization & Analysis from Curtin University. The authors also acknowledge the support from the 2019 Youth Innovative Talents Project by Education Department of Guangdong Province (2018GkQNCX018), the Technology Program of Shenzhen City (JCYJ20180305164033934) and the project of Civil Aviation Flight University of China (J2020-048), the Sichuan Science and Technology Program Project (2020YJ0501).

References

1 J. A. Schuler, H. Yokokawa, C. F. Calderone, Q. Jeangros, Z. Wuillemin, A. Hessler-Wyser and J. Van Herle, *J. Power Sources*, 2012, **201**, 112–120.
2 K. Pei, Y. C. Zhou, K. Xu, Z. Y. He, Y. Chen, W. L. Zhang, S. Yoo, B. T. Zhao, W. Yuan, M. L. Liu and Y. Chen, *Nano Energy*, 2020, **72**, 104704.
3 J. Zhou, J. M. Yang, Z. Zong, L. Fu, Z. J. Lian, C. S. Ni, J. K. Wang, Y. H. Wan and K. Wu, *J. Power Sources*, 2020, **468**, 228349.
4 X. Yang, R. Y. Li, Y. Yang, G. L. Wen, D. Tian, X. Y. Lu, Y. Z. Ding, Y. H. Chen and B. Lin, *J. Alloys Compd.*, 2020, **831**, 154711.
5 Y. Q. Li, L. Y. Na, Z. Lu and S. X. Li, *Int. J. Hydrogen Energy*, 2020, **45**, 15650–15657.
6 C. C. Wang, K. Chen and S. P. Jiang, *J. Electrochem. Soc.*, 2014, **161**, F1133–F1139.
7 C. C. Wang, K. Chen, T. Jiang, Y. Yang, Y. Song, H. Meng, S. P. Jiang and B. Lin, *Electrochim. Acta*, 2018, **269**, 188–195.
8 H. Yokokawa, *ECS Trans.*, 2017, **78**, 2211–2221.
9 M. Kornely, N. H. Menzler, A. Weber and E. Ivers-Tiffee, *Fuel Cells*, 2013, **13**, 506–510.
10 T. Horita, D. H. Cho, F. Wang, M. Nishi, T. Shimonosono, H. Kishimoto, K. Yamaji, M. E. Brito, H. Yokokawa, *Fuel Cell Seminar 2012*, 2013, vol. 51, pp. 69–77.
11 S.-N. Lee, A. Atkinson and J. A. Kilner, *J. Electrochem. Soc.*, 2013, **160**, F629–F635.
12 S. P. Jiang and X. Chen, *Int. J. Hydrogen Energy*, 2014, **39**, 505–531.
13 L. Zhao, J. Drennan, C. Kong, S. Amarasinghe and S. P. Jiang, *J. Mater. Chem. A*, 2014, **2**, 11114–11123.
14 C. C. Wang, S. Darvish, K. Chen, B. Hou, Q. Zhang, Z. Tan, Y. Zhong and S. P. Jiang, *Electrochim. Acta*, 2019, 202–212.
15 K. Chen, J. Hyodo, L. Zhao, N. Ai, T. Ishihara and S. P. Jiang, *J. Electrochem. Soc.*, 2013, **160**, F1033–F1039.
16 K. Chen, N. Ai, L. Zhao and S. P. Jiang, *J. Electrochem. Soc.*, 2013, **160**, F183–F190.
17 S. P. Jiang, J. P. Zhang and X. G. Zheng, *J. Eur. Ceram. Soc.*, 2002, **22**, 361–373.
18 B. Wei, K. Chen, C. C. Wang, Z. Lü and S. P. Jiang, *Solid State Ionics*, 2015, **281**, 29–37.
19 C. C. Wang, K. O'Donnell, L. Jian and S. P. Jiang, *J. Electrochem. Soc.*, 2015, **162**, F507–F512.
20 E. Bucher, C. Gspan, F. Hofer and W. Sitte, *Solid State Ionics*, 2013, **238**, 15–23.